Study on the Resistance Distribution at the Contact between Molybdenum Disulfide and Metals

Yao Guo, Yuxiang Han, Jiapeng Li,[†] An Xiang, Xianlong Wei, Song Gao, and Qing Chen*

Key Laboratory for the Physics and Chemistry of Nanodevices, Department of Electronics, Peking University, Beijing 100871, People's Republic of China.
[†]Present address: Department of Electronic and Computer Engineering, Hong Kong University of Science and Technology, Kowloon, Hong Kong.

ABSTRACT Contact resistance hinders the high performance of electrical devices, especially devices based on two-dimensional (2D) materials, such as graphene and transition metal dichalcogenide. To engineer contact resistance, understanding the resistance distribution and carrier transport behavior at the contact area is essential. Here, we developed a method that can be used to obtain some key parameters of contact, such as transfer length (L_t), sheet resistance of the 2D materials beneath the contacting metal (R_{sh}), and contact resistivity between the 2D materials and the metal electrode (ρ_c). Using our method, we studied the contacts between molybdenum disulfide (MoS_2) and metals, such as titanium and gold, in bilayer and few-layered MoS_2 devices. Especially, we found that R_{sh} is obviously larger than the sheet resistance of the same 2D materials in the channel (R_{ch}) in all the devices we studied. With the increasing of the back-gate voltage, L_t increases and R_{sh}, ρ_c, R_{ch}, and the contact resistance R_c decrease in all the devices we studied. Our results are helpful for understanding the metal—MoS_2 contact and improving the performances of MoS_2 devices.

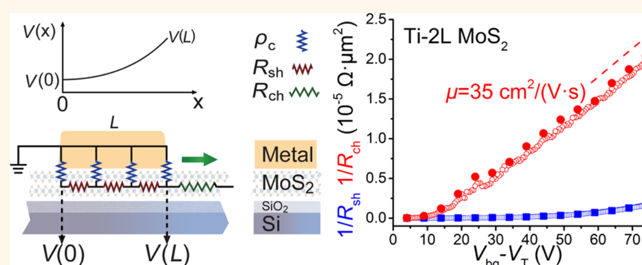

KEYWORDS: MoS_2 · FET · contact resistance · two-dimensional materials · transfer length

Along with the scaling down of electronic devices, contact resistance is playing a more and more important role in circuit resistance and hinders the high performance of circuits.[1] After decades of engineering on the metal—Si contact, the contact resistance of silicon-based devices has been lowered to an acceptable level.[2] Two-dimensional (2D) materials, such as graphene and transition metal dichalcogenides, have fascinating properties in some aspects and show great potential in future electronic devices.[3−5] Field effect transistors (FETs) based on molybdenum disulfide (MoS_2) have been demonstrated to have several impressive characteristics, such as an ON/OFF current ratio as high as 10^8, reasonable electron mobility up to hundreds of $cm^2/(V \cdot s)$, a subthreshold swing approaching the theoretical limit of 60 mV/dec at room temperature, and atomically thin layered structure, suppressing short-channel effects.[4,6−8] However, the metal—MoS_2 contact resistance (R_c) is up to 5 kΩ·μm to 1 MΩ·μm, which is more than 30 times larger than that of the metal—Si contact.[8,9] Such a high contact resistance blocks further performance optimization regardless of the efforts on enhancing the carrier mobility or scaling the channel length.[10,11]

So far, the origin of large metal—MoS_2 contact resistance is unclear. Several possible explanations have been proposed: the wide contact tunnel barrier at the interface blocking electron tunneling between the metal and MoS_2, the large layer-to-layer resistance between MoS_2 layers, and the Schottky barrier related to the work function of the contacting metal.[7,9,12−15] Using a contacting metal with a low work function, molecular doping and a thin interlayer "insulation" barrier have been reported to lower the effective Schottky barrier.[7,16−18] However, to the best of our knowledge, acceptable contact resistance for high-performance devices has not been reported, yet there is much more work to do to pave the way to the utilization of MoS_2 as an electronic material. To further engineer metal—MoS_2 contact, a deep understanding of the resistance distribution and carrier transport behavior at the contact area is urgently needed.

* Address correspondence to qingchen@pku.edu.cn.

Received for review February 15, 2014 and accepted July 17, 2014.

Published online July 17, 2014
10.1021/nn503152r

© 2014 American Chemical Society

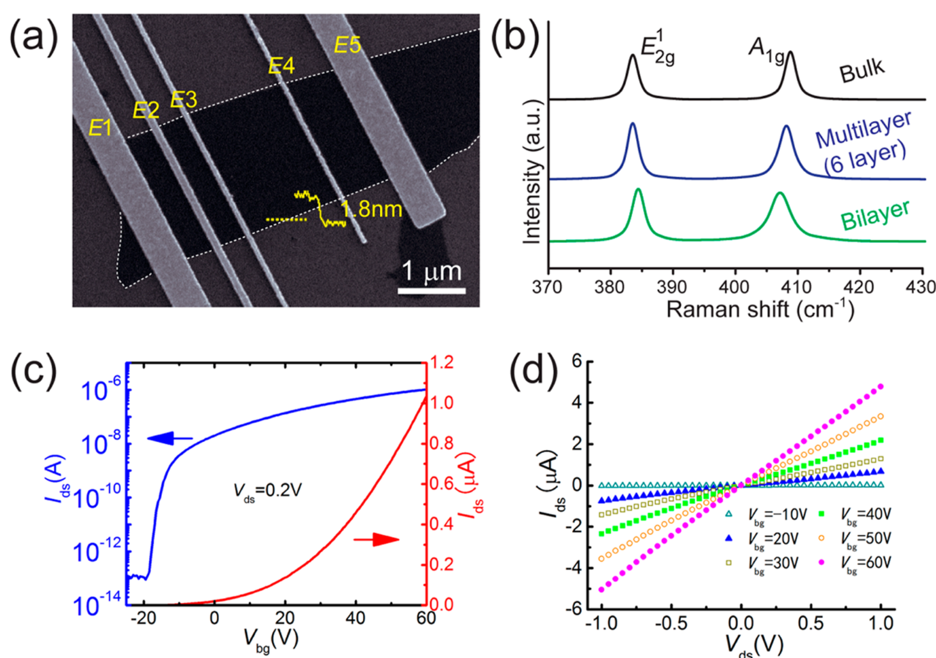

Figure 1. (a) SEM image of the Ti−2L MoS_2 device. The MoS_2 sheet has darker contrast compared to the substrate and is outlined by the white dotted line. The metal electrodes were marked from *E*1 to *E*5. A height difference between the MoS_2 sheet and the substrate obtained by AFM is marked. (b) Raman spectrum of a bulk MoS_2, the 2L MoS_2 in (a), and a 6L MoS_2. Transfer (c) and output (d) characteristics of the 2L MoS_2 FET, using *E*1, *E*5, and the substrate as the source, drain, and back-gate electrodes.

Here we discuss metal−MoS_2 contact particularly. Different from the generally used four-probe method and transfer length method to obtain contact resistance, we develop a method to study the detailed resistance distribution at contact area. Through experimental measurements, we obtain some key parameters of the contacts between MoS_2 and metals, such as titanium (Ti) and gold (Au). Our results are helpful for understanding and reducing the contact resistance of metal−MoS_2 contact.

RESULTS AND DISCUSSION

As shown in Figure 1a, five electrodes were fabricated to contact the same individual MoS_2 sheet on a SiO_2/Si substrate, marked as *E*1, *E*2, *E*3, *E*4, and *E*5. The MoS_2 sheet shown in Figure 1a has two layers (2L), confirmed by atomic force microscopy (AFM) study and Raman spectrum (Figure 1b).[19] The electrode materials of the 2L MoS_2 device shown in Figure 1a are 5 nm Ti/65 nm Au. The transfer and output characteristics of this device were measured using *E*1, *E*5, and the Si substrate as the source, drain, and back-gate electrodes. As shown in Figure 1c and d, the results agree well with those in the literature.[4] The threshold voltage (V_T) is −14 V, extracted using the second derivative of $\ln(I_{ds})$ method.[20] The $I_{ds}-V_{ds}$ curves are symmetric and linear within the measuring range. The electrical characteristic of the device is observed to be stable, and repeated measurements provide reproducible results. In addition to this bilayer MoS_2 (2L MoS_2) device with Ti−2L MoS_2 contact, seven devices with similar structure based on multilayer MoS_2 (ML MoS_2) with Ti−ML MoS_2 contact (four devices) and Au−ML MoS_2 contact (three devices) were also fabricated and successfully studied. The data measured from a Ti−6L MoS_2 device and a Au−6L MoS_2 device are shown in Supporting Information I. We choose Ti and Au as examples of contact metals because Ti has a lower work function, while Au has a higher work function.

We consider the metal−MoS_2 contact in MoS_2 FETs as that shown in Figure 2a. ρ_c is the contact resistivity of the metal−MoS_2 contact. R_{sh} and R_{ch} are the sheet resistance of the MoS_2 sheet beneath the contact and in the channel, respectively. Note that in the conventional transfer length method R_{sh} and R_{ch} are treated as being identical based on the assumptions that the metal−semiconductor contact is a completely "diffusive" one and the sheet resistance under the metal is not affected significantly by the metal. However, these assumptions, especially the second one, may not be valid in the contact between 2D materials and metals.[21] Here, for the first time to the best of our knowledge, we treat R_{sh} and R_{ch} as being different in the metal−MoS_2 contact.

When a metal electrode is grounded, the potential of the electrode is 0. According to Ohm's law and Kirchhoff's law, we have

$$dV(x)/dx = I(x)R_{sh}/W \quad (1)$$

$$dI(x)/dx = WV(x)/\rho_c \quad (2)$$

where $V(x)$ is the potential of the MoS_2 sheet beneath the metal, $I(x)$ is the current in the MoS_2 sheet along the *x* direction, and *W* is the width of the contact. Here, ρ_c and R_{sh} are assumed to be independent of $V(x)$ at small

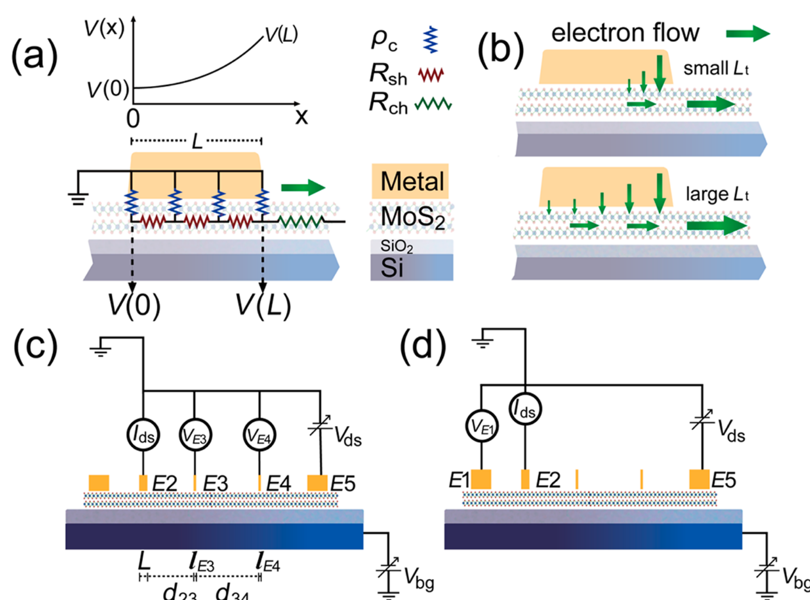

Figure 2. (a) Schematic diagram showing the contact resistance model we used. (b) Schematic diagrams of the current distribution with small (upper diagram) and large (lower diagram) L_t. (c) Schematic circuit diagram for measuring V_{E3}, V_{E4}, and I_{ds}. (d) Schematic circuit diagram for measuring V_{E1} and I_{ds}.

V_{ds}; this assumption is confirmed to be reasonable by our results obtained below that R_c is independent of V_{ds}. Note that for metal–ML MoS_2 contact, ρ_c is an effective contact resistivity rather than the absolute resistivity of the metal–MoS_2 interface, because carriers transport through several MoS_2 layers as well as the metal–MoS_2 interface along the sheet normal direction.[9] The coupled equations have simple solutions considering the boundary condition that $I(x)$ is zero at $x = 0$. For an electrode with length L (as shown in Figure 2a), we have

$$V(L) = V(0)\cosh(L\sqrt{R_{sh}/\rho_c}) \tag{3}$$

$$V(L)/I(L) = \sqrt{R_{sh}\rho_c}\coth(L\sqrt{R_{sh}/\rho_c})/W \tag{4}$$

where $V(0)$ is the potential of the MoS_2 sheet at $x = 0$, $V(L)$ is the potential of the MoS_2 sheet at $x = L$, and $I(L)$ is the current of the MoS_2 sheet at $x = L$. From another point of view, as the metal electrode is grounded, $V(L)$ equals the voltage drop on the whole contact, and $I(L)$ is the current going out of the contact and flowing through the channel between the source and drain. Therefore, $I(L) = I_{ds}$ and the contact resistance is

$$R_c = V(L)/I_{ds} \tag{5}$$

Transfer length,

$$L_t = \sqrt{\rho_c/R_{sh}} \tag{6}$$

is a parameter that describes the effective conductive length of the contact near the channel. As shown in Figure 2b, for small L_t, current crowds around the edge of the contact, while for large L_t, more contact area is involved in the current transport.[22,23]

The resistance distribution at the contact area of $E2$ is studied through the measurements using the circuits schematically shown in Figure 2c and d. In the measurements, $E2$ was grounded and used as the source, $E5$ was used as the drain, the Si substrate was used as the back gate, and $E1$, $E3$, and $E4$ were used as voltage probes. One type of measurement (noted as M1) was performed as follows: at a fixed source–drain voltage $V_{ds} = 0.2$ V, the back-gate voltage (V_{bg}) was swept with a step of 0.5 V in a range, such as from −10 V to +60 V, electrical parameters I_{ds}, V_{E3}, and V_{E4} were measured as shown in Figure 2c, and I_{ds} and V_{E1} were measured as shown in Figure 2d. Besides such measurement, we also performed another type of measurement (noted as M2) as follows: at a fixed V_{bg}, we swept V_{ds} from −1 V to 1 V and measured I_{ds}, V_{E1}, V_{E3}, and V_{E4} as shown in Figure 2c and d, and then changed V_{bg} step by step with each step being 5 V and measured the above parameters again. The results obtained from M1 and M2 are consistent (as shown together in Figures 3–5), indicating our results are reliable. When the length of $E2$ (L, varies from 104 to 130 nm among different devices in the present work) is comparable to the transfer length L_t of the contact, $V(0)$ equals the measured voltage of electrode $E1$, V_{E1}. Otherwise, if $L \gg L_t$, $V(0)$ drops close to 0 and could not be measured. That is the reason that we elaborately designed the length of electrode $E2$. More detailed discussion on the accuracy and reliability of the above measurements is given in Supporting Information II.

With the data obtained from the above measurements, the resistance distribution of $E2$ can be obtained, but the calculation is not simple. Normally, the effect of voltage probes is neglected. However, neglecting the effect of $E3$ and $E4$ may cause a large error in the present case, because the length of the voltage probes, $E3$ and $E4$, is comparable to the transfer length

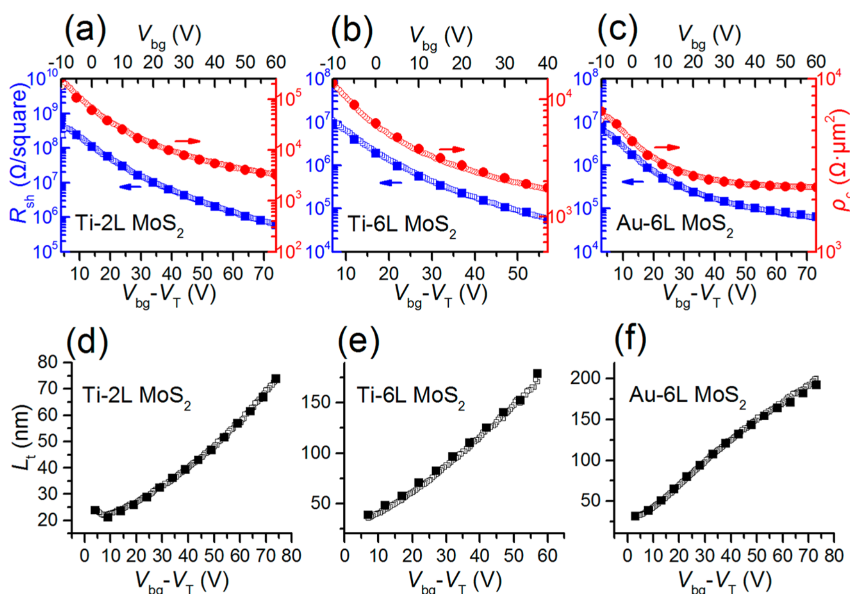

Figure 3. Change of R_{sh} and ρ_c as a function of V_{bg} for the Ti−2L MoS_2 contact (a), the Ti−6L MoS_2 contact (b), and the Au−6L MoS_2 contact (c). Change of L_t as a function of V_{bg} for the Ti−2L MoS_2 contact (d), the Ti−6L MoS_2 contact (e), and the Au−6L MoS_2 contact (f). In these figures, the hollow marks were obtained through M1; the solid marks were obtained through M2.

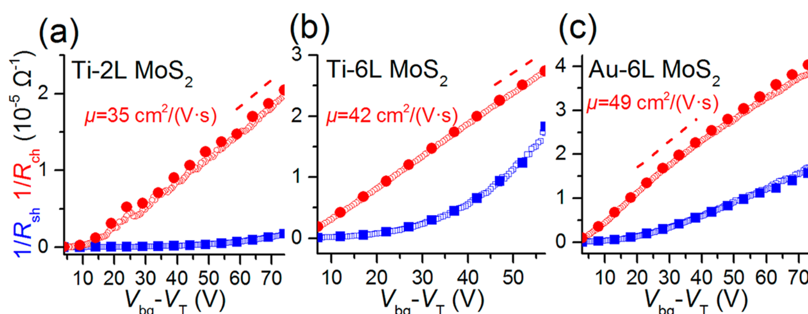

Figure 4. Comparison of $1/R_{ch}$ (red spheres) and $1/R_{sh}$ (blue squares) of the Ti−2L MoS_2 device (a), the Ti−6L MoS_2 device (b), and the Au−6L MoS_2 device (c). In these figures, the hollow marks were obtained through M1; the solid marks were obtained through M2.

L_t, as confirmed later. In such a case, current may go into the metal and flow back to the MoS_2 across the contact area of the voltage probes during our measurements (shown in Supporting Information III, Figure S4). Therefore, we considered the effect of $E3$ and $E4$ during our calculations. Assuming R_{sh} and ρ_c are the same for all the contacts, considering the boundary condition that $I(x) = I_{ds}$ on both the left and the right sides of a voltage probe with length l, and taking into account that the potential of $E3$ and $E4$ is not zero, the voltage drop from one side to the other side of a voltage probe, $\Delta V(l)$, is

$$\Delta V(l) = 2I_{ds}\sqrt{R_{sh}\rho_c}\tanh\left(\frac{l}{2}\sqrt{R_{sh}/\rho_c}\right)/W \quad (7)$$

The detailed process to derive this equation is given in Supporting Information III. Also,

$$V_{E3} - V(L) = \Delta V(l_{E3})/2 + I_{ds}R_{ch}d_{23}/W \quad (8)$$

$$V_{E4} - V_{E3} = \Delta V(l_{E3})/2 + \Delta V(l_{E4})/2 + I_{ds}R_{ch}d_{34}/W \quad (9)$$

where $\Delta V(l_{E3})$ and $\Delta V(l_{E4})$ are the voltage drop across $E3$ and $E4$, and l_{E3} and l_{E4} are the length of $E3$ and $E4$, respectively. We can further simplify the equations as follows. From eqs 3 and 4, we obtain

$$V(0)\cosh(L\sqrt{R_{sh}/\rho_c}) = I_{ds}\sqrt{R_{sh}\rho_c}\coth(L\sqrt{R_{sh}/\rho_c})/W \quad (10)$$

From eqs 3, 7, and 8, we obtain

$$V_{E3} - V(0)\cosh(L\sqrt{R_{sh}/\rho_c}) = \frac{I_{ds}}{W}\left[\sqrt{R_{sh}\rho_c}\tanh\left(\frac{l_{E3}}{2}\sqrt{R_{sh}/\rho_c}\right) + R_{ch}d_{23}\right] \quad (11)$$

From eqs 7 and 9, we obtain

$$V_{E4} - V_{E3} = \frac{I_{ds}}{W}\left[\sqrt{R_{sh}\rho_c}\tanh\left(\frac{l_{E3}}{2}\sqrt{R_{sh}/\rho_c}\right) + \sqrt{R_{sh}\rho_c}\tanh\left(\frac{l_{E4}}{2}\sqrt{R_{sh}/\rho_c}\right) + R_{ch}d_{34}\right] \quad (12)$$

Using eqs 10−12, knowing the geometric parameters of the devices measured by scanning electron microscopy (SEM) and the measured I_{ds}, V_{E1}, V_{E3}, and V_{E4}, we can numerically calculate R_{sh}, ρ_c, and R_{ch} through iteration.

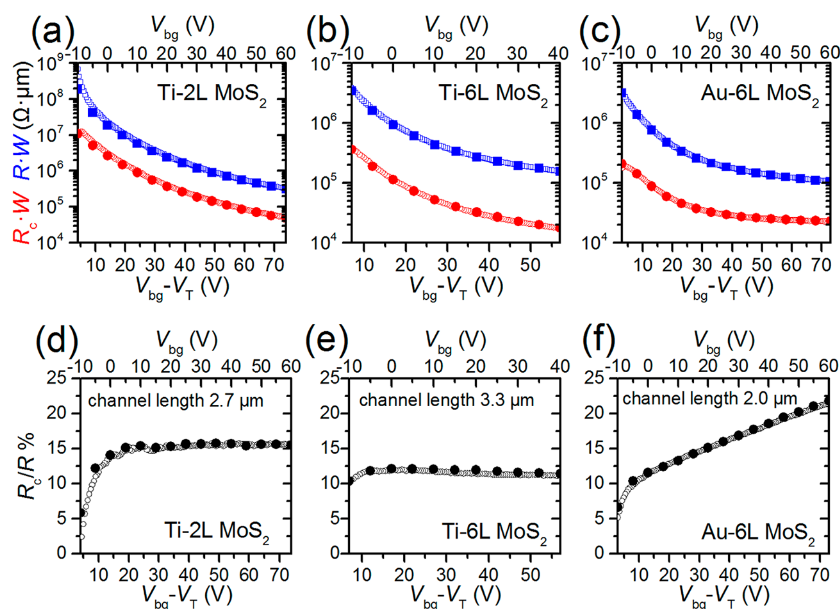

Figure 5. Contact resistance R_c of *E*2 and the whole device resistance *R* of the Ti−2L MoS_2 device (a), the Ti−6L MoS_2 device (b), and the Au−6L MoS_2 device (c). Proportion of contact resistance R_c in the whole resistance *R* of the Ti−2L MoS_2 device (d), the Ti−6L MoS_2 device (e), and the Au−6L MoS_2 device (f). In these figures, the hollow marks were obtained through M1; the solid marks were obtained through M2.

The contact resistance R_c and the transfer length L_t can then be obtained using eqs 5 and 6.

Figure 3a−c show R_{sh} and ρ_c we obtained at different gate voltage in three typical devices, with Ti−2L MoS_2, Ti−6L MoS_2, and Au−6L MoS_2 contacts, respectively. It can be seen that both R_{sh} and ρ_c drop severely with increasing V_{bg} in all three contacts, being consistent with previous reports[14] as well as the expectation considering the accumulation of electrons in the MoS_2 layer at large V_{bg}. R_{sh} drops more severely than ρ_c as $V_{bg} - V_T$ increases in all three types of contacts. We observed that both R_{sh} and ρ_c are more sensitive to the number of layers than to the contacting metals. It is observed that both R_{sh} and ρ_c in the Ti−2L MoS_2 contact are obviously larger than those in the Ti−6L MoS_2 and Au−6L MoS_2 contacts at the same $V_{bg} - V_T$. One of the reasons might be attributed to the rise of the conduction band bottom in the band structure as the layer number of MoS_2 decreases.[24] In the same $V_{bg} - V_T$ range, both R_{sh} and ρ_c drop more severely in the Ti−2L MoS_2 contact than in the Ti−6L MoS_2 and Au−6L MoS_2 contacts. Comparing the contacts between 6L MoS_2 and different metals (Ti and Au), R_{sh} does not differ a lot, but ρ_c is obviously different. The smallest ρ_c we obtained (which is 1.8 k$\Omega \cdot \mu$m^2 in Ti−6L MoS_2 when $V_{bg} - V_T = 57$ V) is obviously larger than that in the best metal−graphene contact reported in the literature.[25]

We observed that L_t increases with the gate voltage in most of the cases in all the contacts, as shown in Figure 3d−f. This is because R_{sh} drops more severely than ρ_c as $V_{bg} - V_T$ increases (shown in Figure 3a−c). For the Ti−2L MoS_2 contact, L_t is only 24 nm when $V_{bg} - V_T = 4$ V, indicating that a rather limited area of the contact is involved in electron transmission. L_t increased from 24 to 74 nm as $V_{bg} - V_T$ increases from 4 V to 74 V, indicating a relief of current crowding and the broadening of the effective current path; more carriers go a longer distance along the contact in the MoS_2 layers before transferring into the metal or reverse at larger V_{bg}. L_t of the Ti−6L MoS_2 contact is larger than that of the Ti−2L MoS_2 contact at the same gate voltage and increases from 39 nm to 179 nm as $V_{bg} - V_T$ increases from 7 V to 57 V. L_t of the Au−6L MoS_2 contact is roughly the same as that of the Ti−6L MoS_2 contact at the same gate voltage and increases from 31 nm to 192 nm as $V_{bg} - V_T$ increases from 3 V to 73 V. The fact that we obtained consistent results from eight devices (shown in Supporting Information IV, Figure S5) supports the reliability of our method. Previous work on a CVD monolayer MoS_2 sheet has also found that current flows not only at the edge of the metal contact but also in the metal contact area with a large contact length.[14] However, L_t is larger than 600 nm in that report and decreases with the back-gate voltage. As we treat R_{sh} and R_{ch} as being different, the present R_{sh} and L_t are not exactly the same as those in the literature.

In Figure 4, the sheet conductance of the MoS_2 sheet beneath the metal electrode ($1/R_{sh}$) is compared with that of the channel ($1/R_{ch}$) for three typical devices. In all the devices we studied, $1/R_{sh}$ is obviously smaller than $1/R_{ch}$ in the whole voltage range we studied (the difference at low gate voltage can be seen clearly when the data are presented in the logarithmic coordinates in Supporting Information V, Figure S6), indicating that

the property of the atomically thin MoS_2 sheets has been changed after contacting the metal electrode. For the 2L MoS_2 device, $1/R_{sh}$ is more than 1 order of magnitude smaller than $1/R_{ch}$ in almost the whole V_{bg} range we measured. While for the 6L MoS_2 device, the difference between $1/R_{sh}$ and $1/R_{ch}$ decreased at high V_{bg}. In previous studies on the transfer length L_t at the contact between 2D materials and metals, R_{sh} and R_{ch} are normally treated as being the same.[23,26] However, our present results show that R_{sh} and R_{ch} of thin MoS_2 are different, especially when the thickness of the materials is atomically thin.

The conductivity degeneration of the materials beneath the contacting metal might be due to the following reasons. Impurities and defects might be introduced to the MoS_2 sheets at the contact area when metal electrodes were fabricated. Defects have been reported to lower the contact resistivity between the metal and MoS_2;[27,28] however, they may increase carrier scattering and increase R_{sh}. As both ρ_c and R_{sh} contribute to the contact resistance, the defects may need to be engineered to obtain the smallest R_c. Strain might be introduced to the MoS_2 sheets at the contact area by the contacting metals and change the electrical properties of the MoS_2 sheets, and inhomogeneous strain could introduce additional carrier scattering.[29−31] The metal with a large work function might reduce the electron density in the MoS_2 layers.[7] The metal could also change the dielectric environment of the MoS_2 sheets and partially screen the effect of the back-gate voltage. Due to the large charge screening length of MoS_2 ($\lambda_{MoS_2} = 7$ nm),[9] the screening of the metal could have a significant effect on the ability of the back-gate voltage to modulate the electron density in the MoS_2 sheet contacting the metal. Raman peak shifts have been observed on MoS_2 after it was deposited by thin Pd, Au, and Ag films.[29] We also observed Raman peak shifts caused by Ti and Au thin films as shown in Supporting Information VI, Figure S7, supporting that the property of the atomically thin MoS_2 sheets has been changed after contacting the metal. More work is under way to understand these Raman peak shifts.

Carrier mobility μ was also extracted from the data shown in Figure 4 considering $d(1/R_{ch}) = \mu C_{ox}\, d(V_{bg} - V_T)$, where C_{ox} is the capacity per unit area of the 300 nm silicon oxide. Note that the present extracted mobility is the property of the channel on the substrate, while the field effect mobility normally extracted from the transfer curve of a device is affected by the existence of contact resistance. The carrier mobility extracted from the present devices has a reasonable value.

The contact resistance R_c of *E*2 in the three typical devices is compared with the total resistance $R = V_{ds}/I_{ds}$ in Figure 5. For a better comparison among different devices, normalized R_c, R_cW, is presented in Figure 5a−c. Both R_c and R decrease as V_{bg} increases in all three devices, similar to R_{ch} (as shown in Figure 4), indicating the gate voltage modulates the contact as well as the channel in the ON state we studied. Previous work on a CVD monolayer MoS_2 sheet reported that the contact resistance (R_c) decreases by more than 2 orders as V_{bg} increased about 100 V.[14] Here, we observed that R_c in the Ti−2L MoS_2 device decreases by more than 2 orders of magnitude when V_{bg} increases by about 70 V. However, R_c in the Ti−6L MoS_2 device decreases by less than 1.5 orders of magnitude as V_{bg} increases by about 50 V, and R_c in the Au−6L MoS_2 device decreases by about 1 order of magnitude as V_{bg} increases by about 70 V.

Although R_{sh} is obviously larger than R_{ch}, as the channel length in the present devices is at least 1 order of magnitude longer than L_t, R_c is still a small part in the total resistance R, being less than 17% of R in the Ti−2L MoS_2 device, about 10−12% of R in the Ti−6L MoS_2 device, and less than 23% in the Au−6L MoS_2 device in the whole V_{bg} range we studied (as shown in Figure 5d−f). The fraction of R_c in R in the Ti−MoS_2 devices increases with gate voltages at low $V_{bg} - V_T$ and then remains roughly the same when $V_{bg} - V_T >$ 20 V in the 2L MoS_2 device and $V_{bg} - V_T > 15$ V in the 6L MoS_2 device. In the Au−6L MoS_2 device, the fraction of R_c in R increases rapidly with gate voltage at low $V_{bg} - V_T$ and then increases slowly but linearly with gate voltage when $V_{bg} - V_T > 10$ V. In all these devices, if the channel length decreases to a couple hundred nanometers, the fraction of R_c in R could increase to be the main part of R, as has been shown in previous reports.[10] Therefore, it is crucial to reduce R_c to achieve high performance in short-channel devices.

Until now we obtain a resistance distribution using thin electrodes with their length comparable to the transfer length. This method takes advantage of the potential distribution of the 2D materials beneath a thin electrode and measures the electrical characteristics of the contact directly. The method is also applicable for other metal−2D material contact with large L_t.

On the basis of the present results, we discuss some key strategies to reduce metal−MoS_2 contact resistance. First, the length of the contact electrodes must be larger than L_t. For a contact with $L \gg L_t$, eq 4 degenerates to $R_c = (R_{sh}\rho_c)^{1/2}/W$. Thus, reducing ρ_c and R_{sh} are the two key ways to reduce R_c. Most of the previous work studying metal−MoS_2 contact has focused on reducing ρ_c, such as engineering the work function and band alignment and processing annealing.[7,8] Our results show that R_{sh} also plays an importance part in constituting contact resistance, and reducing R_{sh} is equally important in engineering the contact resistance. Several methods have been used to reduce R_c, probably through reducing R_{sh}. A gentle metal deposition process and cleaning method might reduce the defects and impurities in MoS_2 introduced in the device fabrication process. As R_{sh} of the metal−ML MoS_2 contact is less affected than the metal−2L MoS_2 contact, ML MoS_2

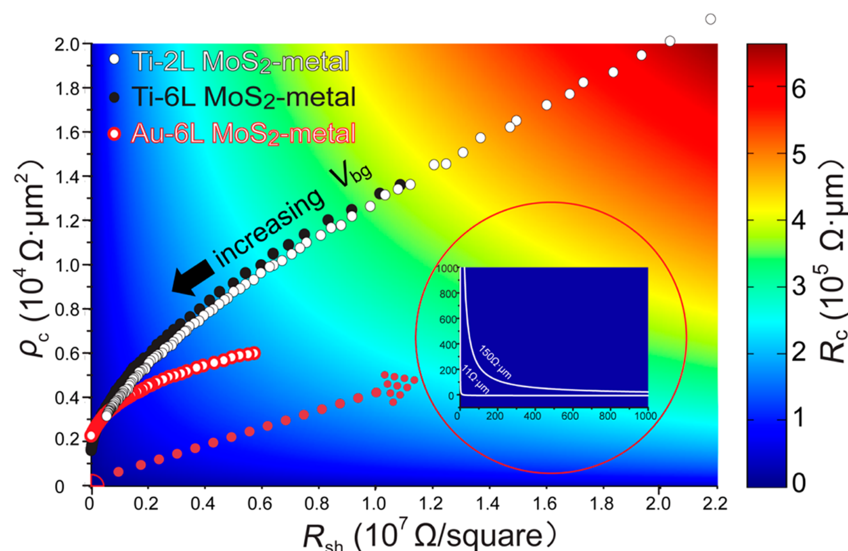

Figure 6. Color map of R_c *versus* ρ_c and R_{sh}. The target contour lines for R_c = 150 Ω·μm (metal–Si contact) and R_c = 11 Ω·μm (metal–graphene contact) are enlarged and shown within the circle.

is more preferable to make low contact resistance devices. Engineering the dielectric environment may also improve the contact. Recently, an interlayer between MoS_2 layers and a metal has also been demonstrated to improve contact effectively.[17,32] Such an interlayer might also protect the MoS_2 sheets from being damaged in the device fabrication process. As shown in the color map of R_c in Figure 6, increasing V_{bg} could effectively reduce both ρ_c and R_{sh}. The three types of metal–MoS_2 contacts follow a similar trend with increasing V_{bg}. However, there is still a long way toward the target of R_c = 150 Ω·μm (the value of the metal–Si contact) as well as R_c = 11 Ω·μm (the best value of the metal–graphene contact).

CONCLUSIONS

In summary, we developed a method to obtain a resistance distribution using narrow electrodes with length comparable to the transfer length. The method is also applicable for other metal–2D material contact with large L_t. Through this method, we studied the detailed resistance distribution in metal–MoS_2 contacts in the ON-state devices. For the first time to the best of our knowledge, we treat the sheet resistance of the MoS_2 sheet beneath the electrode (R_{sh}) and that in the channel (R_{ch}) as being different in the metal–MoS_2 contact. Similar to that in the literature, both R_{sh} and R_{ch} decrease with increasing gate voltage. However, R_{sh} is obviously larger than R_{ch} in all the metal–MoS_2 contacts (such as Ti–2L MoS_2, Ti–6L MoS_2, and Au–6L MoS_2 contacts) in the whole gate voltage range we studied, indicating the MoS_2 in the contact area has been changed by contacting the metal electrode, while the amount of difference between R_{sh} and R_{ch} is different in various metal–MoS_2 contacts and at different gate voltage.

Both ρ_c and R_{sh} decrease with increasing gate voltage, but R_{sh} drops more severely, so that L_t increases with increasing $V_{bg} - V_T$, indicating a relief of current crowding and the broadening of the effective current path at large V_{bg}. L_t of the metal–6L MoS_2 contact is larger than that of the Ti–2L MoS_2 contact at the same V_{bg}. In the Ti–2L MoS_2 contact, L_t is only 24 nm when $V_{bg} - V_T$ = 4 V. The largest L_t we obtained is 218 nm for the Au–5L MoS_2 contact when $V_{bg} - V_T$ is 72 V.

As the channel length of the present devices is much longer than L_t, the contact resistance R_c is less than 23% of the total resistance of the circuit R in all the devices we studied. However, R_c could be the main part of R in short-channel devices.

METHODS

Device Fabrication. MoS_2 sheets were exfoliated onto a heavily doped silicon wafer covered by 300 nm of silicon dioxide. Rectangular sheets with homogeneous contrast were selected under an optical microscope.[33] Two-layered photoresist (copolymer plus PMMA) and electron beam lithography were used to define the electrodes. A metal film of 5 nm Ti/65 nm Au was deposited to form the Ti–MoS_2 contact, and 0.3 nm Ti/70 nm Au was deposited to form the Au–MoS_2 contact by an electron beam evaporator. The length of *E*2 was elaborately designed to be comparable with the transfer length in our experiment. After lift-off in acetone, the wafer was immediately transferred into a vacuum chamber with four probes for electrical characterization with a Keithley 4200 semiconductor characterization system.

Characterization. AFM and Raman spectra were used to characterize the thickness and layer number of the MoS_2 sheets.[19,34] A laser with a 488 nm wavelength was used for the Raman spectrum study. The geometric parameters of the devices, including W, L, d_{23}, d_{34}, l_{E3}, and l_{E4}, were all measured by SEM. The parameters of the three typical devices are listed in Table 1.

TABLE 1. Geometric Parameters and V_T of the Three Typical Devices

		electrode length (nm)					distance between electrodes (μm)		width (μm)	threshold voltage (V)
metal	no. of MoS_2 layers	*E1*	*E2*	*E3*	*E4*	*E5*	d_{23}	d_{34}	W	V_T
Ti	2	490	117	65	53	490	0.44	1.5	1.9	−14
Ti	6	500	112	65	50	500	0.45	2	2.4	−17
Au	6	510	115	112	111	510	0.44	0.99	2.5	−13

Once the devices had been fabricated, the electrical measurements were performed immediately using the circuits schematically shown in Figure 2c and d. The gate voltage range was chosen so that the devices were in the ON state.

Conflict of Interest: The authors declare no competing financial interest.

Acknowledgment. We thank Prof. Shimin Hou, Dr. Jianbo Yin, Mr. Chenguang Qiu, and Mr. Jiapei Shu for valuable discussions. This work was supported by the MOST (2012CB932702, 2010CB934203) and the NSF of China (11374022, 61321001).

Supporting Information Available: SEM images and electrical characteristics of the Ti−6L MoS_2 device and the Au−6L MoS_2 device, analysis on the reliability of the electrical measurements, evaluation of the effect of the voltage probes *E3* and *E4*, L_t of eight metal−MoS_2 contacts, comparison of $1/R_{ch}$ and $1/R_{sh}$ in logarithmic coordinates, Raman spectroscopy study of MoS_2 sheets before and after metal deposition. This material is available free of charge *via* the Internet at http://pubs.acs.org.

REFERENCES AND NOTES

1. Leonard, F.; Talin, A. A. Electrical Contacts to One- and Two-Dimensional Nanomaterials. *Nat. Nanotechnol.* **2011**, *6*, 773–783.
2. Zhang, S. L.; Östling, M. Metal Silicides in CMOS Technology: Past, Present, and Future Trends. *Crit. Rev. Solid State Mater. Sci.* **2003**, *28*, 1–129.
3. Schwierz, F. Graphene Transistors. *Nat. Nanotechnol.* **2010**, *5*, 487–496.
4. Radisavljevic, B.; Radenovic, A.; Brivio, J.; Giacometti, V.; Kis, A. Single-Layer MoS_2 Transistors. *Nat. Nanotechnol.* **2011**, *6*, 147–150.
5. Schwierz, F. Graphene Transistors: Status, Prospects, and Problems. *Proc. IEEE* **2013**, *101*, 1567–1584.
6. Yoon, Y.; Ganapathi, K.; Salahuddin, S. How Good Can Monolayer MoS_2 Transistors Be? *Nano Lett.* **2011**, *11*, 3768–3773.
7. Das, S.; Chen, H. Y.; Penumatcha, A. V.; Appenzeller, J. High Performance Multilayer MoS_2 Transistors with Scandium Contacts. *Nano Lett.* **2012**, *13*, 100–105.
8. Baugher, B. W. H.; Churchill, H. O. H.; Yang, Y.; Jarillo-Herrero, P. Intrinsic Electronic Transport Properties of High-Quality Monolayer and Bilayer MoS_2. *Nano Lett.* **2013**, *13*, 4212–4216.
9. Das, S.; Appenzeller, J. Where Does the Current Flow in Two-Dimensional Layered Systems? *Nano Lett.* **2013**, *13*, 3396–3402.
10. Liu, H.; Neal, A. T.; Ye, P. D. Channel Length Scaling of MoS_2 MOSFETs. *ACS Nano* **2012**, *6*, 8563–8569.
11. Radisavljevic, B.; Kis, A. Mobility Engineering and a Metal−Insulator Transition in Monolayer MoS_2. *Nat. Mater.* **2013**, *12*, 815–820.
12. Popov, I.; Seifert, G.; Tománek, D. Designing Electrical Contacts to MoS_2 Monolayers: A Computational Study. *Phys. Rev. Lett.* **2012**, *108*, 156802.
13. Monch, W. Valence-Band Offsets and Schottky Barrier Heights of Layered Semiconductors Explained by Interface-Induced Gap States. *Appl. Phys. Lett.* **1998**, *72*, 1899–1901.
14. Liu, H.; Si, M.; Deng, Y.; Neal, A. T.; Du, Y.; Najmaei, S.; Ajayan, P. M.; Lou, J.; Ye, P. D. Switching Mechanism in Single-Layer Molybdenum Disulfide Transistors: An Insight into Current Flow across Schottky Barriers. *ACS Nano* **2014**, *8*, 1031–1038.
15. Gong, C.; Colombo, L.; Wallace, R. M.; Cho, K. The Unusual Mechanism of Partial Fermi Level Pinning at Metal-MoS_2 Interfaces. *Nano Lett.* **2014**, *14*, 1714–1720.
16. Du, Y. C.; Liu, H.; Neal, A. T.; Si, M. W.; Ye, P. D. Molecular Doping of Multilayer MoS_2 Field-Effect Transistors: Reduction in Sheet and Contact Resistances. *IEEE Electron Device Lett.* **2013**, *34*, 1328–1330.
17. Chen, J. R.; Odenthal, P. M.; Swartz, A. G.; Floyd, G. C.; Wen, H.; Luo, K. Y.; Kawakami, R. K. Control of Schottky Barriers in Single Layer MoS_2 Transistors with Ferromagnetic Contacts. *Nano Lett.* **2013**, *13*, 3106–3110.
18. Fang, H.; Chuang, S.; Chang, T. C.; Takei, K.; Takahashi, T.; Javey, A. High-Performance Single Layered WSe_2 p-FETs with Chemically Doped Contacts. *Nano Lett.* **2012**, *12*, 3788–3792.
19. Li, H.; Zhang, Q.; Yap, C. C. R.; Tay, B. K.; Edwin, T. H. T.; Olivier, A.; Baillargeat, D. From Bulk to Monolayer MoS_2: Evolution of Raman Scattering. *Adv. Funct. Mater.* **2012**, *22*, 1385–1390.
20. Ortiz-Conde, A.; García Sánchez, F. J.; Liou, J. J.; Cerdeira, A.; Estrada, M.; Yue, Y. A Review of Recent MOSFET Threshold Voltage Extraction Methods. *Microelectron. Reliab.* **2002**, *42*, 583–596.
21. Xia, F.; Perebeinos, V.; Lin, Y. M.; Wu, Y.; Avouris, P. The Origins and Limits of Metal-Graphene Junction Resistance. *Nat. Nanotechnol.* **2011**, *6*, 179–184.
22. Grosse, K. L.; Bae, M.-H.; Lian, F.; Pop, E.; King, W. P. Nanoscale Joule Heating, Peltier Cooling and Current Crowding at Graphene-Metal Contacts. *Nat. Nanotechnol.* **2011**, *6*, 287–290.
23. Nagashio, K.; Nishimura, T.; Kita, K.; Toriumi, A. Contact Resistivity and Current Flow Path at Metal/Graphene Contact. *Appl. Phys. Lett.* **2010**, *97*, 143514.
24. Mak, K. F.; Lee, C.; Hone, J.; Shan, J.; Heinz, T. F. Atomically Thin MoS_2: A New Direct-Gap Semiconductor. *Phys. Rev. Lett.* **2010**, *105*, 136805.
25. Robinson, J. A.; LaBella, M.; Zhu, M.; Hollander, M.; Kasarda, R.; Hughes, Z.; Trumbull, K.; Cavalero, R.; Snyder, D. Contacting Graphene. *Appl. Phys. Lett.* **2011**, *98*, 053103.
26. Venugopal, A.; Colombo, L.; Vogel, E. M. Contact Resistance in Few and Multilayer Graphene Devices. *Appl. Phys. Lett.* **2010**, *96*, 013512.
27. McDonnell, S.; Addou, R.; Buie, C.; Wallace, R. M.; Hinkle, C. L. Defect-Dominated Doping and Contact Resistance in MoS_2. *ACS Nano* **2014**, *8*, 2880–2888.
28. Liu, D.; Guo, Y.; Fang, L.; Robertson, J. Sulfur Vacancies in Monolayer MoS_2 and Its Electrical Contacts. *Appl. Phys. Lett.* **2013**, *103*, 183113.
29. Gong, C.; Huang, C.; Miller, J.; Cheng, L.; Hao, Y.; Cobden, D.; Kim, J.; Ruoff, R. S.; Wallace, R. M.; Cho, K.; *et al.* Metal Contacts on Physical Vapor Deposited Monolayer MoS_2. *ACS Nano* **2013**, *7*, 11350–11357.
30. Hui, Y. Y.; Liu, X.; Jie, W.; Chan, N. Y.; Hao, J.; Hsu, Y.-T.; Li, L.-J.; Guo, W.; Lau, S. P. Exceptional Tunability of Band Energy in a Compressively Strained Trilayer MoS_2 Sheet. *ACS Nano* **2013**, *7*, 7126–7131.
31. Johari, P.; Shenoy, V. B. Tuning the Electronic Properties of Semiconducting Transition Metal Dichalcogenides by Applying Mechanical Strains. *ACS Nano* **2012**, *6*, 5449–5456.
32. Dankert, A.; Langouche, L.; Kamalakar, M. V.; Dash, S. P. High-Performance Molybdenum Disulfide Field-Effect

Transistors with Spin Tunnel Contacts. *ACS Nano* **2014**, *8*, 476–482.
33. Benameur, M. M.; Radisavljevic, B.; Héron, J. S.; Sahoo, S.; Berger, H.; Kis, A. Visibility of Dichalcogenide Nanolayers. *Nanotechnology* **2011**, *22*, 125706.
34. Lee, C.; Yan, H.; Brus, L. E.; Heinz, T. F.; Hone, J.; Ryu, S. Anomalous Lattice Vibrations of Single- and Few-Layer MoS_2. *ACS Nano* **2010**, *4*, 2695–2700.